

Effects of friction stir processing and minor Sc addition on the microstructure, mechanical properties, and damping capacity of 7055 Al alloy

Y. Chen^a, C.Y. Liu^{a,b,*}, B. Zhang^c, Z.Y. Ma^{b,**}, W.B. Zhou^d, H.J. Jiang^a, H.F. Huang^a, L.L. Wei^a

^a Key Laboratory of New Processing Technology for Nonferrous Metal & Materials, Ministry of Education, Guilin University of Technology, Guilin 541004, China

^b Shenyang National Laboratory for Materials Science, Institute of Metal Research, Chinese Academy of Sciences, 72 Wenhua Road, Shenyang 110016, China

^c State Key Laboratory of Metastable Materials Science and Technology, Yanshan University, Qinhuangdao 066004, China

^d Anlan Aluminium Co., Ltd., Nanning 530000, China

ARTICLE INFO

Keywords:

Al alloy
Microstructure
Damping capacity
Mechanical properties

ABSTRACT

This study investigated the effects of friction stir processing (FSP) and addition of 0.25% (mass ratio) Sc on the microstructure, mechanical properties, and damping capacity of AA 7055 alloy. Microstructure analyses revealed that a low tool rotation rate of 300 rpm effectively inhibited the grain coarsening in the recrystallization of the alloy during FSP. Sc addition prevented the coarsening of grains and precipitated η phase and the annihilation of dislocations in the FSP AA 7055 alloy. After being subjected to FSP at 300 rpm, the AA 7055 alloy containing Sc exhibited good mechanical and damping properties, which were mainly attributed to the fine recrystallized grain structure, fine precipitated η phase, and large number of nano-sized $\text{Al}_3(\text{Sc}, \text{Zr})$ particles located at the grain boundaries and dislocations. This work provides an effective strategy for preparing commercial Al alloys with excellent damping capacity and mechanical properties.

1. Introduction

In recent years, researchers have attempted to develop metallic materials with high damping and mechanical properties for application to special active control devices in modern industries [1,2].

Given their low density and excellent mechanical properties, Al–Zn–Mg(Cu) series (7xxx) alloys are one of the most important structural materials used in numerous fields, including aviation, aerospace, and civilian transport [3–7]. However, commercial Al alloys, including 7xxx Al alloys, are low-damping materials. Thus, the damping capacity of 7xxx Al alloys must be improved to extend their engineering applications.

Our previous investigation demonstrated that the damping capacity of Al–35Zn alloy can be significantly improved through optimization of grain structures by reducing the grain size, promoting the formation of equiaxed grains, and introducing a wetting interface between the Al and Zn phases [8]. Luo et al. [9] found that the excellent damping capacity of metals was due to the grain structures with excellent grain boundary (GB) sliding capacity. As such, the damping capacity of 7xxx Al alloys can be enhanced by improving the GB sliding capacity.

Ma et al. [10,11] and Kang et al. [12] reported that 7xxx Al alloys can achieve excellent GB sliding capacity when subjected to friction stir processing (FSP) primarily because of the equiaxed fine grain structure of these alloys. Hence, FSP may be an effective strategy for improving the damping capacity of 7xxx Al alloys. In addition, FSP Al alloys exhibited excellent mechanical properties, such as high strength and toughness, which were attributed to the GB strengthening mechanism and the excellent GB sliding capacity, respectively [10–15].

Liu et al. [13] reported that a FSP Sc-containing Al–Mg alloy exhibited a more excellent GB sliding capacity than that of other FSP Al alloys. This characteristic was mainly attributed to the grain refining effect of Sc on Al alloys during deformation. Moreover, Sc addition has been proven effective for refining the grains of 7xxx Al alloys [16–18].

Primary $\text{Al}_3(\text{Sc}, \text{Zr})$ phases can serve as heterogeneous nucleation sites for Al grains during solidification to induce grain refinement [19]. Furthermore, the $\text{Al}_3(\text{Sc}, \text{Zr})$ particles that precipitated during homogenization can strongly pin the GBs during subsequent deformation and consequently promote grain refinement [16–18]. Therefore, Sc addition may also be another effective strategy for improving the damping capacity of the 7xxx Al alloys without sacrificing their mechanical

* Correspondence to: C.Y. Liu, Key Laboratory of New Processing Technology for Nonferrous Metal & Materials, Ministry of Education, Guilin University of Technology, Guilin 541004, China.

** Corresponding author.

E-mail addresses: lcy261@glut.edu.cn (C.Y. Liu), zya@imr.ac.cn (Z.Y. Ma).

<https://doi.org/10.1016/j.matchar.2017.11.030>

Received 16 July 2017; Received in revised form 27 October 2017; Accepted 12 November 2017

Available online 13 November 2017

1044-5803/ © 2017 Elsevier Inc. All rights reserved.

Table 1
Chemical composition of the 7055 and 7055-0.25Sc alloys.

	Zn	Mg	Cu	Zr	Sc
7055	7.82	1.95	2.24	0.16	–
7055-0.25Sc	7.81	1.93	2.24	0.16	0.25

properties. However, no study has investigated on the damping behavior of Sc-containing 7xxx Al alloys after FSP.

This study investigated the effects of FSP and Sc addition on the microstructure, mechanical properties, and damping capacity of 7055 alloys. The aim was to fabricate 7xxx Al alloys with excellent damping capacity and mechanical properties via FSP and Sc addition.

2. Experimental Methods

This study used 3 mm-thick rolled sheets of 7055 and 7055 containing 0.25% (mass ratio) Sc (7055-0.25Sc) alloys. The chemical compositions of these two alloys are shown in Table 1. The sheets were subjected to solution treatment at 470 °C for 2 h and then water quenched (defined as SS).

FSP was conducted at a constant traverse speed of 100 mm min⁻¹ with different tool rotation rates of 300 and 1500 rpm, which were denoted as FSP-300 and FSP-1500, respectively. A tool with a concave shoulder (diameter: 10 mm) and a taper threaded pin (length: 2.7 mm; diameter: 5 mm) were used.

The microstructures of the samples were examined by optical microscopy (OM), electron backscattered diffraction (EBSD), and transmission electron microscopy (TEM, JEM-2010). EBSD measurements were performed using a Hitachi S-3400N-II scanning electron microscope. The films for TEM were ground to a thickness of 50 μm and thinned using a twinjet electropolishing device.

The tensile tests were conducted on an Instron-3369-type testing machine at a strain rate of 4 × 10⁻⁴ s⁻¹. The specimens were machined in parallel to the FSP direction. The fracture surfaces resulting from the tensile tests were observed by scanning electron microscopy (SEM, S-4800).

The internal friction behavior (i.e., damping performance) of the samples was characterized using specimens with dimensions of 1.2 mm × 4 mm × 25 mm. Internal friction tests were conducted with a dynamic mechanical analyzer (Q800, TA) under single-cantilever mode. Measurements were obtained at a strain amplitude (ϵ) of 1 × 10⁻⁴, a frequency (f) of 1 Hz, and temperatures (T) ranging from 50 °C to 380 °C at a heating rate of 5 °C/min.

3. Results

Fig. 1 shows the microstructures of the SS 7055 and 7055-0.25Sc

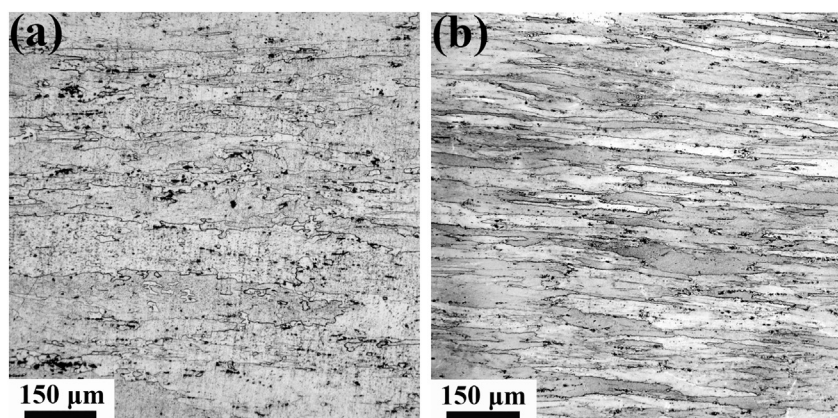


Fig. 1. OM micrographs of SS (a) 7055 and (b) 7055-0.25Sc alloys.

alloys obtained by OM. After solid solution treatments, the SS 7055 alloy displayed an incompletely recrystallized structure composed of elongated deformed grains and recrystallized equiaxed grains (Fig. 1a), whereas the SS 7055-0.25Sc alloy was characterized by a fibrous rolling deformation structure (Fig. 1b). Compared with the SS 7055 alloy, the SS 7055-0.25Sc alloy exhibited a smaller grain size.

Fig. 2 shows the microstructures of the SS 7055 and 7055-0.25Sc alloys obtained by TEM. Equiaxed particles with a size range of 20–30 nm were observed in the 7055 alloy (Fig. 2a). These particles were considered the Al₃Zr phase on the basis of the chemical composition and heat treatment process [20]. Compared with the SS 7055 alloy, the SS 7055-0.25Sc alloy exhibited a considerably higher density of nano-sized particles (Fig. 2b). The chemical composition, heat treatment process, and selected area of diffraction (SAD) indicated that the nano-sized particles in the 7055-0.25Sc alloy after solution treatment were the Al₃(Sc,Zr) phase.

Figs. 3 and 4 respectively show the microstructures and grain size distributions of the FSP 7055 and 7055-0.25Sc alloys obtained by EBSD. Completely recrystallized grains with equiaxed shape were observed in all FSP samples (Fig. 3). The FSP-300 samples exhibited a multi-scale grain structure composed of fine grains (as fine as 0.8 μm) and coarse grains (larger than 20 μm). The average grain size (AGS) of the FSP-300 7055 alloy was approximately 3.6 μm (Figs. 3a and 4a). The FSP-300 7055-0.25Sc alloy exhibited a lower proportion of large grains compared with that of the FSP-300 7055 alloy, and the largest grain of this sample was approximately 10 μm. The AGS of the FSP-300 7055-0.25Sc alloy was approximately 1.7 μm (Figs. 3b and 4b). When the rotation rate was increased to 1500 rpm, the recrystallized grains of the FSP samples became coarsened and more uniformly distributed. The AGSs of the FSP-1500 7055 and 7055-0.25Sc alloys were approximately 5.2 (Figs. 3c and 4c) and 2.8 μm (Figs. 3d and 4d), respectively.

Fig. 5 shows the microstructures of the FSP 7055 alloys obtained by TEM. SAD revealed that both Al₃Zr and η phases were obtained in the FSP-300 7055 alloy. Al₃Zr particles were observed in the precipitated η phase in both samples, and this phenomenon was also observed in the 7055 alloy after heat treatment [20]. Compared with the FSP-300 7055 alloy (Fig. 5a), the FSP-1500 7055 alloy exhibited a larger η phase (Fig. 5b).

Fig. 6 shows the microstructures of the FSP 7055-0.25Sc alloys obtained by TEM. Precipitated η phases were observed in the FSP 7055-0.25Sc alloys, and their size did not significantly increase with increasing rotation rate (Fig. 6a and b). Compared with the FSP-1500 7055 alloy (Fig. 5b), the FSP-1500 7055-0.25Sc alloy exhibited a smaller η phase (Fig. 6b). In addition, large numbers of nano-sized Al₃(Sc,Zr) particles were observed in the FSP 7055-0.25Sc alloys, of which some were located at GBs (Fig. 6c) and dislocations (Fig. 6d).

Fig. 7 depicts the stress–strain curves of the SS, FSP 7055, and 7055-0.25Sc alloys. The mechanical properties of the samples are provided in Table 2. The strengths of the 7055 and 7055-0.25Sc alloys decreased as

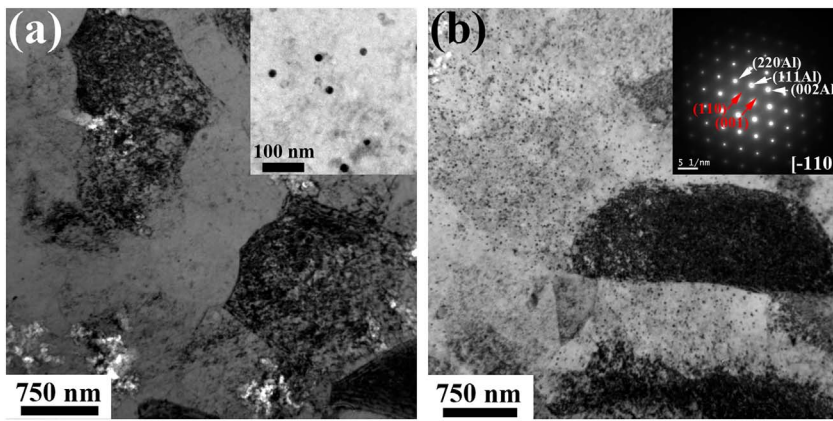


Fig. 2. TEM micrographs of SS (a) 7055 and (b) 7055-0.25Sc alloys. The inset in (a) is the high magnification, and the inset in (b) is the selected area of diffraction, and the red numbers correspond to the planes of $\text{Al}_3(\text{Sc,Zr})$. (For interpretation of the references to colour in this figure legend, the reader is referred to the web version of this article.)

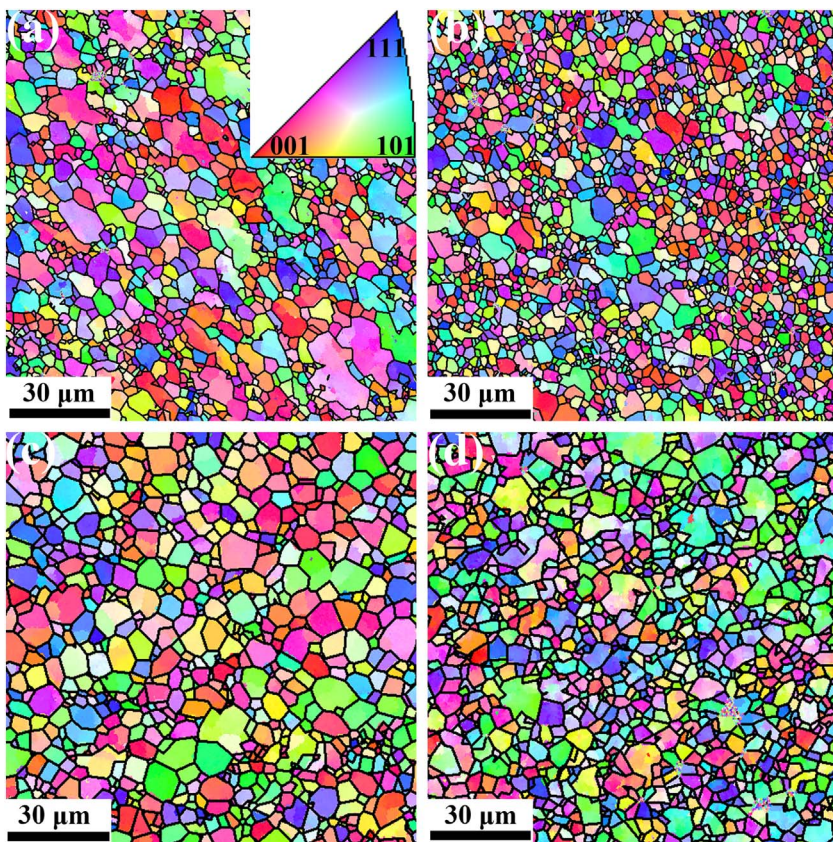


Fig. 3. EBSD maps showing the grain structure of FSP-300 (a) 7055 and (b) 7055-0.25Sc alloys, and FSP-1500 (c) 7055 and (d) 7055-0.25Sc alloys.

the heat input was increased during FSP. By contrast, the ductility of these two alloys exhibited an opposite trend with increasing heat input. The UTS of the FSP-1500 7055 alloy was 41 MPa lower than that of the FSP-300 7055 alloy, whereas the UTS of the FSP-1500 7055-0.25Sc alloy was only 12 MPa lower than that of the FSP-300 7055-0.25Sc alloy. These findings indicated that the FSP 7055-0.25Sc alloy exhibited a higher thermal stability of microstructures during FSP at a high rotation rate. The 7055-0.25Sc alloys exhibited a higher strength and ductility than the 7055 alloys under the same processing conditions. Compared with the other FSP samples, the FSP-300 7055-0.25Sc alloy displayed balanced mechanical properties, including higher strength and reasonable ductility.

Fig. 8 shows the variations of damping capacity with temperature for the SS, FSP 7055, and 7055-0.25Sc alloys. The damping capacities of all samples were improved with increasing temperature. The temperature-dependent damping capacities of the SS 7055 and 7055-0.25Sc alloys were improved by FSP, and the FSP-300 samples

exhibited a higher damping capacity than the FSP-1500 samples (Figs. 8a and b). Moreover, the 7055-0.25Sc alloys exhibited a higher damping capacity than the 7055 alloys under the same processing conditions (Fig. 8c).

4. Discussion

Nano-sized Al_3Zr and $\text{Al}_3(\text{Sc,Zr})$ phases were formed in the 7055 and 7xxx-Sc alloys during homogenization treatment, and these phases can pin the GBs during subsequent rolling and solution treatments [16–18,20]. The density of the $\text{Al}_3(\text{Sc,Zr})$ phase in the 7055-0.25Sc alloy was significantly higher than that of Al_3Zr in the 7055 alloy (Fig. 2). Thus, more fine grains were retained in the SS 7055-0.25Sc alloy (Fig. 1).

FSP can refine the grains of 7055 and 7055-0.25Sc alloys, and decreasing the rotation rate has been proven effective in reducing the heat input during FSP [21,22]. Therefore, FSP with 300 rpm inhibited the

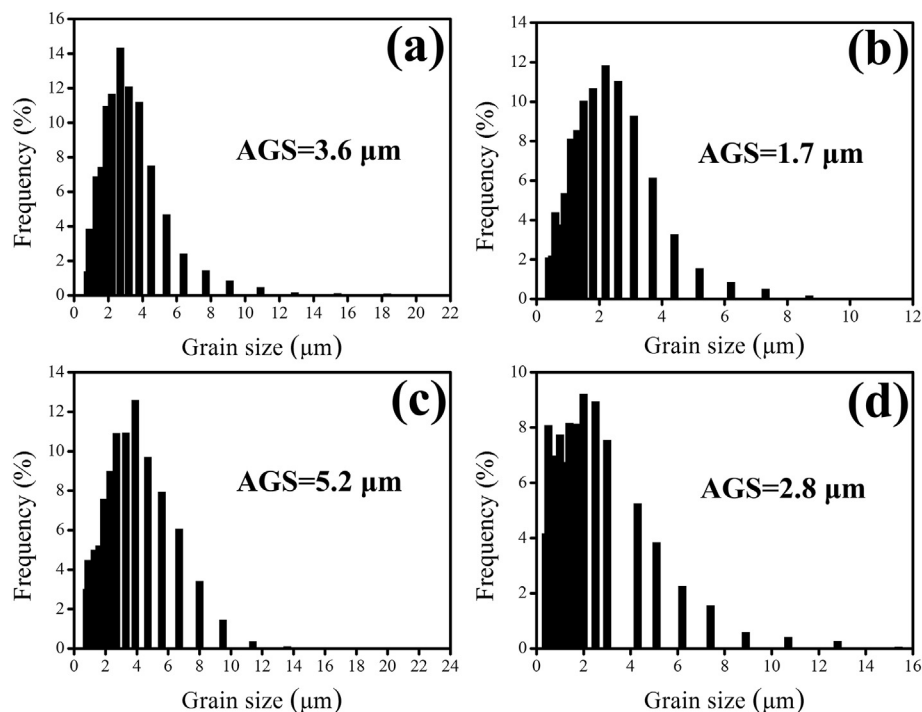


Fig. 4. Grain size distributions of FSP-300 (a) 7055 and (b) 7055-0.25Sc alloys, and FSP-1500 (c) 7055 and (d) 7055-0.25Sc alloys.

coarsening of recrystallized grains in these two alloys (Fig. 3).

The high temperature during FSP led to the precipitation in the 7055 and 7055-0.25Sc alloys, and the nano-sized particles provided preferential nucleation sites for precipitates because of the high interfacial energy. Thus, GP zones precipitated in the Al_3Zr particles in the FSP 7055 alloys. Then, the increase in the friction-induced temperature transformed the GP zones into η phase. Consequently, Al_3Zr particles were observed on the precipitated η phase (Fig. 5). Increasing the rotation rate can enhance the heat input during FSP [21,22] and therefore further promote the precipitation in the 7055 alloy. Thus, compared with the FSP-300 7055 alloy, the FSP-1500 7055 alloy exhibited a larger η phase (Fig. 5).

Minor Sc addition inhibited the coarsening of the η phase in the 7055 alloy during FSP (Figs. 5 and 6). Using a 3D atom probe, Chen et al. [23] and Jiang et al. [24] found that Sc atoms were segregated at the precipitated phase/Al matrix interfaces in Al–Cu–Sc alloys, and that the growth of the precipitated phase was inhibited by these Sc atoms [23]. In the present study, a large number of Sc atoms was also located at the precipitated η phase/Al matrix interfaces. Thus, the η phase in the 7055-0.25Sc alloy exhibited a high thermal stability during FSP with high heat input, and the size of the η phase was smaller in the FSP-1500 7055-0.25Sc alloy than in the FSP-1500 7055 alloy (Figs. 5b and 6b).

Numerous $\text{Al}_3(\text{Sc}, \text{Zr})$ particles located at the GBs in the 7055-0.25Sc alloys (Figs. 2b and 6c) can strongly pin the GBs during deformation [25,26], thereby preventing intense grain growth (Fig. 3). Therefore, the structure of the FSP 7055-0.25Sc alloy displayed more fine grains. However, the grain growth in the FSP 7055 alloy was not completely suppressed by Sc addition, and this phenomenon was also observed in the other 7xxx Al alloys during friction stir welding (FSW) [25]. FSP or FSW promoted the generation of additional GBs generation in the Al alloys via grain refinement, and the non-uniform distribution of the $\text{Al}_3(\text{Sc}, \text{Zr})$ phase in the Sc-containing 7xxx Al alloys diminished the pinning effect in a number of GBs. Consequently, the grain growth in these alloys was not completely suppressed. Additional dislocations that formed during FSP were also reserved in the FSP 7055-0.25Sc alloy because of the dislocation pinning effect of $\text{Al}_3(\text{Sc}, \text{Zr})$ particles (Fig. 6d).

Compared with the SS samples, the FSP samples exhibited reduced strength (Fig. 7). Microstructure analysis revealed two competing effects of FSP on the strengths of the SS 7055 and 7055-0.25Sc alloys: (i) hardening caused by grain refinement and precipitates; and (ii) softening caused by the decomposition of the supersaturated solid solution. The net effect resulted in decreased strength after FSP.

Increasing the rotation rate led to the coarsening of the grains and

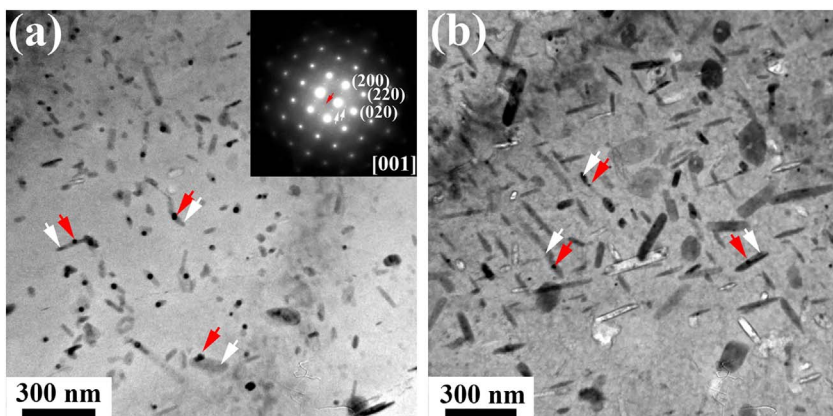


Fig. 5. TEM micrographs of (a) FSP-300 and (b) FSP-1500 7055 alloys. Red arrows denote Al_3Zr particles, and white arrows denote the η phase. The inset in (a) is the selected area of diffraction. Red arrows denote the planes of the Al_3Zr phase, and white arrows denote the planes of the η phase. (For interpretation of the references to colour in this figure legend, the reader is referred to the web version of this article.)

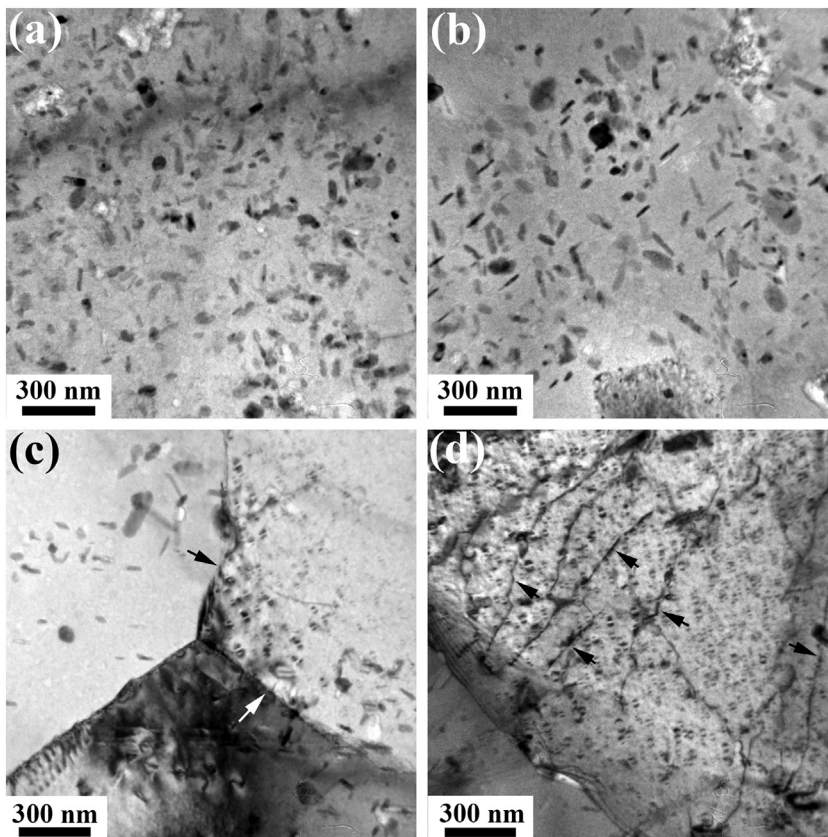


Fig. 6. TEM micrographs of (a) FSP-300 and (b), (c), (d) FSP-1500 7055-0.25Sc alloys. Arrows in (c) denote GBs, and arrows in (d) denote dislocations.

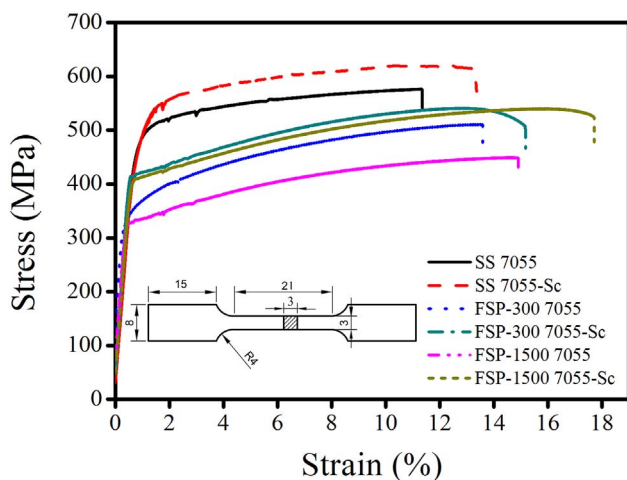


Fig. 7. Stress–strain curves of 7055 and 7055-0.25Sc alloys after solid solution and FSP with various parameters.

Table 2

Tensile properties of 7055 and 7055-0.25Sc alloys after solid solution treatment and FSP with various parameters (YS: yield strength; UTS: ultimate tensile strength; EL: tensile elongation).

		YS (MPa)	UTS (MPa)	EL (%)
SS	7055	467	576	11
	7055-0.25Sc	470	620	13
FSP-300	7055	337	510	13
	7055-0.25Sc	436	560	15
FSP-1500	7055	328	469	15
	7055-0.25Sc	419	548	18

the precipitated phases, thereby decreasing the strength of the FSP samples. However, for the FSP 7055-0.25Sc alloys, the FSP-1500 sample exhibited a slightly lower strength than the FSP-300 sample because of the high thermal stability of the structure (Fig. 6). FSP effectively inhibited the coarsening of the grains and the η phases as well as the annihilation of dislocations in the 7055-0.25Sc alloys because of the pinning effects of the $\text{Al}_3(\text{Sc},\text{Zr})$ particles and the Sc atoms (Fig. 6). Thus, compared with the FSP 7055 alloy, the FSP 7055-0.25Sc alloy under the same FSP conditions exhibited a higher strength because of the higher GB, precipitation, and dislocation strengthening.

Compared with the SS samples, the FSP samples exhibited higher ductility (Fig. 7), which was mainly attributed to the more homogenous microstructures of the latter. In view of the homogenous microstructures in the FSP samples, the redistribution of the stresses during tension prevented strain localization [27], thereby achieving a considerable elongation before failure.

For alloys with fine grain structure, dislocations can be annihilated at GBs, resulting in the accumulation of few dislocations inside the grain interior during deformation. Such alloys always exhibit a low work hardening capacity and poor ductility [28]. FSP with high heat input resulted in grain coarsening, thereby improving the dislocation storage capacity of the FSP samples. Nano-sized $\text{Al}_3(\text{Sc}, \text{Zr})$ particles, which can pin dislocations, also improved the dislocation storage capacity. Thus, the FSP-1500 samples exhibited higher ductility than the FSP-300 samples, and the ductility of the 7055-0.25Sc alloys was higher than that of the 7055 alloys under the same processing condition.

Continuous heating promoted GB sliding and improved the damping capacities of the samples (Fig. 8). Both FSP and Sc addition promoted the grain refinement of the 7055 alloy, and a fine grain structure always contributed to an excellent GB sliding capacity [10–15]. Thus, the temperature-dependent damping capacity of the SS 7055 alloy was improved by FSP and Sc addition according to the interfacial damping mechanism [9,29]. Furthermore, nano-sized $\text{Al}_3(\text{Sc},\text{Zr})$ particles, which were located at GBs (Fig. 6c), effectively inhibited the growth of fine

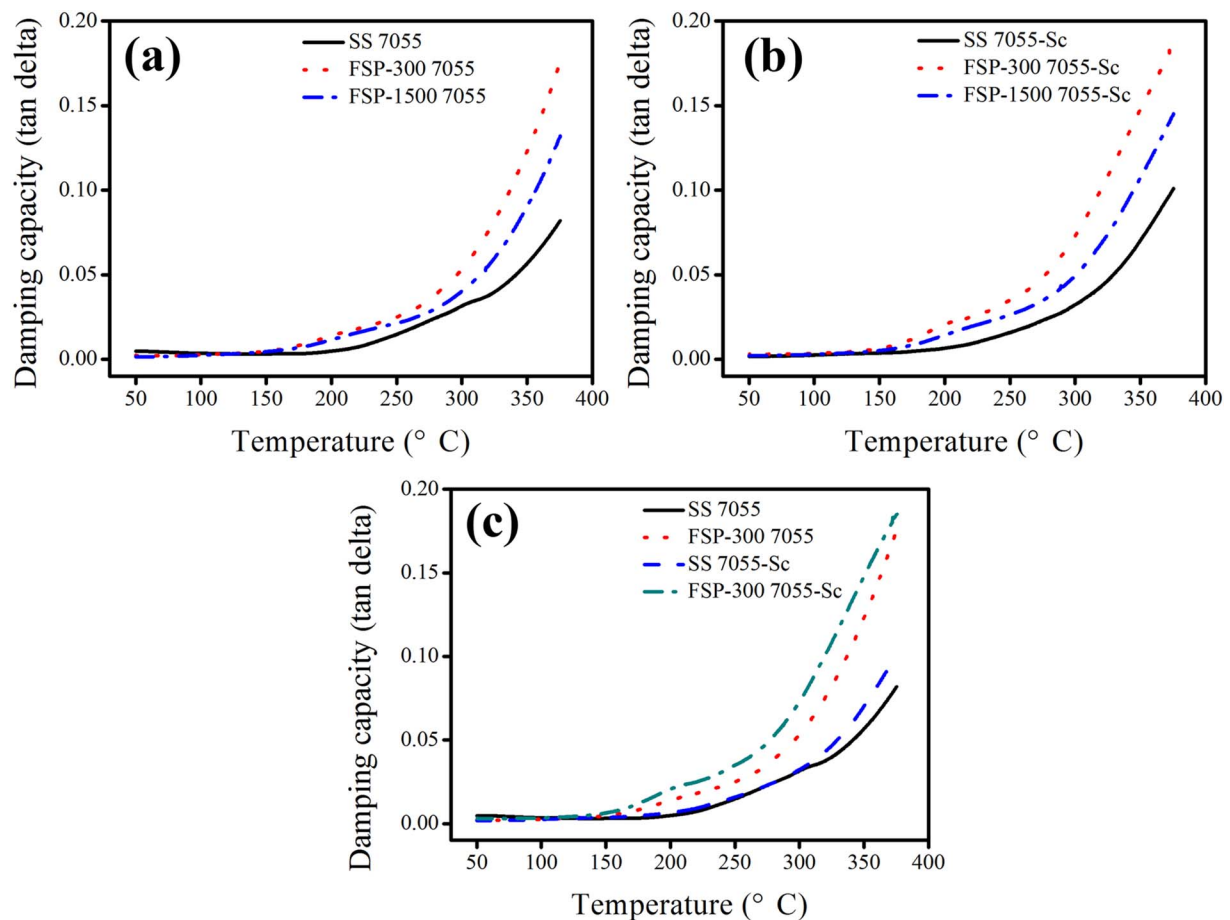


Fig. 8. Temperature-dependent damping capacities of SS and FSP (a) 7055 and (b) 7055-0.25Sc alloys. (c) Comparison of the temperature-dependent damping capacities between the 7055 and 7055-0.25Sc alloys.

grains at high temperature [19]. Thus, the GB sliding capacities of the 7055-0.25Sc alloys were improved during high-temperature damping test, and the FSP-300 7055-0.25Sc alloy exhibited the optimal high-temperature damping capacity.

5. Conclusions

This study demonstrated the potential to achieve good mechanical properties and high damping capacity in 7xxx Al alloys via FSP and Sc addition. The following conclusions were drawn:

- (1) Low tool rotation rate (300 rpm) and minor Sc (0.25%) addition effectively inhibited the grain coarsening in the recrystallization in the 7055 alloy during FSP. An average grain size of approximately 1.7 μm was obtained in the FSP-300 7055-Sc alloy.
- (2) Sc addition effectively inhibited the coarsening of the precipitated η phase and the annihilation of dislocations of the 7055-Sc alloy during FSP with a high tool rotation rate (1500 rpm).
- (3) The FSP 7055-0.25Sc alloys exhibited a higher strength and ductility than the FSP 7055 alloys under the same processing conditions. In addition, compared with the other FSP samples, the FSP-300 7055-0.25Sc alloy displayed balanced mechanical properties, including higher strength and reasonable ductility.
- (4) The temperature-dependent damping capacity of the 7055 alloys was improved by FSP and Sc addition, and the FSP-300 7055-0.25Sc alloy showed the best damping capacity mainly because of its equiaxed fine grain structure.

Acknowledgements

This work was funded by the National Natural Science Foundation of China (No. 51601045), the Guangxi “Bagui” Teams for Innovation and Research, the Guangxi Natural Science Foundation (No. 2015GXNSFBFA139238), and the Research Program of Science and Technology of Guangxi (No. GKAB16380021).

References

- [1] C.F. Zhang, T.X. Fan, W. Cao, D. Zhang, (AlN + Mg₂Si)/Mg composites in situ synthesis and scale effect of particulate on damping capacity, *Mater. Sci. Eng. A* 508 (2009) 190–194.
- [2] S.Q. Chen, X.P. Dong, R. Ma, L. Zhang, H. Wang, Z.T. Fan, Effects of Cu on microstructure, mechanical properties and damping capacity of high damping Mg-1% Mn based alloy, *Mater. Sci. Eng. A* 551 (2012) 87–94.
- [3] D. Wang, D.R. Ni, Z.Y. Ma, Effect of pre-strain and two-step aging on microstructure and stress corrosion cracking of 7050 alloy, *Mater. Sci. Eng. A* 494 (2008) 360–366.
- [4] D. Wang, Z.Y. Ma, Z.M. Gao, Effects of severe cold rolling on tensile properties and stress corrosion cracking of 7050 aluminum alloy, *Mater. Chem. Phys.* 117 (2009) 228–233.
- [5] D. Wang, Z.Y. Ma, Effect of pre-strain on microstructure and stress corrosion cracking of over-aged 7050 aluminum alloy, *J. Alloys Comp.* 469 (2009) 445–450.
- [6] L.L. Wei, Q.L. Pan, H.F. Huang, L. Feng, Y.L. Wang, Influence of grain structure and crystallographic orientation on fatigue crack propagation behavior of 7050 alloy thick plate, *Int. J. Fatigue* 66 (2014) 55–64.
- [7] L.L. Wei, Q.L. Pan, Y.L. Wang, L. Feng, H.F. Huang, Characterization of fracture and fatigue behavior of 7050 aluminum alloy ultra-thick plate, *J. Mater. Eng. Perform.* 22 (2013) 2665–2672.
- [8] H.J. Jiang, C.Y. Liu, Z.Y. Ma, X. Zhang, L. Yu, M.Z. Ma, R.P. Liu, Fabrication of Al-35Zn alloys with excellent damping capacity and mechanical properties, *J. Alloys Compd.* 722 (2017) 138–144.
- [9] B.H. Luo, Z.H. Bai, Y.Q. Xie, The effects of trace Sc and Zr on microstructure and internal friction of Zn-Al eutectoid alloy, *Mater. Sci. Eng. A* 370 (2004) 172–176.
- [10] Z.Y. Ma, F.C. Liu, R.S. Mishra, Superplastic deformation mechanism of an ultrafine-

- grained aluminum alloy produced by friction stir processing, *Acta Mater.* 58 (2010) 4693–4704.
- [11] Z.Y. Ma, F.C. Liu, R.S. Mishra, Superplastic behavior of micro-regions in two-pass friction stir processed 7075Al alloy, *Mater. Sci. Eng. A* 505 (2009) 70–78.
- [12] K. Wang, F.C. Liu, Z.Y. Ma, F.C. Zhang, Realization of exceptionally high elongation at high strain rate in a friction stir processed Al-Zn-Mg-Cu alloy with the presence of liquid phase, *Scripta Mater.* 64 (2011) 572–575.
- [13] F.C. Liu, Z.Y. Ma, L.Q. Chen, Low-temperature superplasticity of Al-Mg-Sc alloy produced by friction stir processing, *Scripta Mater.* 60 (2009) 968–971.
- [14] I. Charit, R.S. Mishra, Low temperature superplasticity in a friction-stir-processed ultrafine grained Al-Zn-Mg-Sc alloy, *Acta Mater.* 53 (2005) 4211–4223.
- [15] Z.Y. Ma, S.R. Sharma, R.S. Mishra, Effect of multiple-pass friction stir processing on microstructure and tensile properties of a cast aluminum-silicon alloy, *Scripta Mater.* 54 (2006) 1623–1626.
- [16] B. Li, Q.L. Pan, X. Huang, Z.M. Yin, Microstructures and properties of Al-Zn-Mg-Mn alloy with trace amounts of Sc and Zr, *Mater. Sci. Eng. A* 616 (2014) 219–228.
- [17] M. Zhang, T. Liu, C.N. He, J. Ding, E.Z. Liu, C.S. Shi, J.J. Li, N.Q. Zhao, Evolution of microstructure and properties of Al-Zn-Mg-Cu-Sc-Zr alloy during aging treatment, *J. Alloys Compd.* 658 (2016) 946–951.
- [18] Y. Deng, Z.M. Yin, J.Q. Duan, K. Zhao, B. Tang, Z.B. He, Evolution of microstructure and properties in a new type 2 mm Al-Zn-Mg-Sc-Zr alloy sheet, *J. Alloys Compd.* 517 (2012) 118–126.
- [19] W.B. Zhou, C.Y. Liu, P.F. Yu, B. Zhang, Z.Y. Ma, K. Luo, M.Z. Ma, R.P. Liu, Effect of scandium on microstructure and mechanical properties of high zinc concentration aluminum alloys, *Mater. Charact.* 127 (2017) 371–378.
- [20] S.D. Liu, X.M. Zhang, M.A. Chen, J.H. You, Influence of aging on quench sensitivity effect of 7055 aluminum alloy, *Mater. Charact.* 59 (2008) 53–60.
- [21] P. Xue, Z.Y. Huang, B.B. Wang, Y.Z. Tian, W.G. Wang, B.L. Xiao, Z.Y. Ma, Intrinsic high cycle fatigue behavior of ultrafine grained pure Cu with stable structure, *Sci. China Mater.* 59 (2016) 531–537.
- [22] P. Xue, B.L. Xiao, Q. Zhang, Z.Y. Ma, Achieving friction stir welded pure copper joints with nearly equal strength to the parent metal via additional rapid cooling, *Scripta Mater.* 64 (2011) 1051–1054.
- [23] B.A. Chen, G. Liu, R.H. Wang, J.Y. Zhang, L. Jiang, J.J. Song, J. Sun, Effect of interfacial solute segregation on ductile fracture of Al-Cu-Sc alloys, *Acta Mater.* 61 (2013) 1676–1690.
- [24] L. Jiang, J.K. Li, G. Liu, R.H. Wang, B.A. Chen, J.Y. Zhang, J. Sun, M.X. Yang, G. Yang, J. Yang, X.Z. Cao, Length-scale dependent microalloying effects on precipitation behaviors and mechanical properties of Al-Cu alloys with minor Sc addition, *Mater. Sci. Eng. A* 637 (2015) 139–154.
- [25] Y. Deng, B. Peng, G.F. Xu, Q.L. Pan, Z.M. Yin, R. Ye, Y.J. Wang, L.Y. Lu, Effects of Sc and Zr on mechanical property and microstructure of tungsten inert gas and friction stir welded aerospace high strength Al-Zn-Mg alloys, *Mater. Sci. Eng. A* 639 (2015) 500–513.
- [26] E. Avtokratova, O. Sitdikov, M. Markushev, R. Mulyukov, Extraordinary high-strain rate superplasticity of severely deformed Al-Mg-Sc-Zr alloy, *Mater. Sci. Eng. A* 538 (2012) 386–390.
- [27] D. Yadav, R. Bauri, Effect of friction stir processing on microstructure and mechanical properties of aluminium, *Mater. Sci. Eng. A* 539 (2012) 85–92.
- [28] Y.T. Zhu, X.Z. Liao, Nanostructured metals: retaining ductility, *Nature Mater.* 3 (2004) 351–352.
- [29] E.J. Lavernia, R.J. Perez, J. Zhang, Damping behavior of discontinuously reinforced ai alloy metal-matrix composites, *Metall. Mater. Trans. A* 26 (1995) 2803–2818.